Acta Crystallographica Section B
Structural Science
ISSN 0108-7681

Synthesis and structural characterization of BaV_4O_9

Thomas Reeswinkel,[a,b] Sebastian Prinz,[a] Karine M. Sparta[a]* and Georg Roth[a]

[a]Institut für Kristallographie der RWTH Aachen, Jägerstrasse 17-19, 52066 Aachen, Germany, and [b]Lehrstuhl für Werkstoffchemie der RWTH Aachen, Kopernikusstrasse 16, 52074 Aachen, Germany

Correspondence e-mail: sparta@xtal.rwth-aachen.de

Received 8 December 2006
Accepted 23 January 2007

The new spin $\frac{1}{2}$ V^{4+} barium oxovanadate BaV_4O_9 was synthesized and studied by means of single-crystal X-ray diffraction. Its room-temperature structure is monoclinic, space group $P2/c$. We discuss the temperature evolution of the crystal structure and thermal expansion tensor of the material between 293 and 100 K.

1. Introduction

Over the last three decades, low-dimensional spin $\frac{1}{2}$ materials have gained considerable importance in condensed matter science because of their exciting physical properties. These comprise, among others, high T_c superconductivity in two-dimensional compounds (Bednorz & Müller, 1986), spin-Peierls transitions and the existence of a spin gap between a singlet ground state and an excited triplet state in one-dimensional antiferromagnets, spin ladders and geometrically frustrated two-dimensional systems. In this context, copper(II) ($S = 1/2$) compounds, such as $CuGeO_3$ (Hase *et al.*, 1993), $Sr_{14}Cu_{24}O_{41}$ (Matsuda & Katsumata, 1996), $SrCu_2O_3$ (Azuma *et al.*, 1994) and $SrCu_2(BO_3)_2$ (Kageyama *et al.*, 1999), have been thoroughly investigated. Among the vanadium(IV) compounds (also $S = 1/2$), CaV_4O_9 was the first two-dimensional spin-gap system discovered (Bouloux & Galy, 1973; Taniguchi *et al.*, 1995). Since then, many other vanadium(IV) compounds were found to exhibit spin-gap behaviour, such as $(VO)_2P_2O_7$ (Johnston *et al.*, 1987), the vanadate family AV_2O_5 with A = Li, Na, Ca, Mg, Ca (Ueda, 1998), $Cs_2V_4O_9$ and $Rb_2V_4O_9$ (Liu & Greedan, 1995) or SrV_4O_9 (Oka *et al.*, 2000); these materials were mostly grown using temperatures between *ca* 1000 and 1500 K. However, barium vanadates containing V^{4+} ions have only been successfully synthesized recently, such as the V^{4+} compounds Ba_2VO_4 (Liu & Greedan, 1993), $Ba_8V_7O_{22}$ (Liu & Greedan, 1994*a*) and $BaVO_3$ (Liu & Greedan, 1994*b*), and the mixed-valence compounds BaV_3O_8 (Oka *et al.*, 1995) and $BaV_7O_{16}\cdot nH_2O$ (Wang *et al.*, 1998). The present work is part of a more general effort to grow new vanadium(IV) compounds under different experimental conditions, in our case with lower growth temperatures *via* a molten salt reaction route. We present the crystal growth and structure determination from single-crystal X-ray diffraction data of BaV_4O_9. Despite the chemical similarity with CaV_4O_9 and SrV_4O_9, this material exhibits a different, and to our knowledge, as yet unknown structure type.[1]

[1] Supplementary data for this paper are available from the IUCr electronic archives (Reference: BM5044). Services for accessing these data are described at the back of the journal.

Table 1
Experimental and refinement details.

Full data can be obtained from the CIF file which has been deposited.

	293 K	250 K	200 K	150 K	100 K
Crystal data					
Chemical formula	BaO_9V_4	BaO_9V_4	BaO_9V_4	BaO_9V_4	BaO_9V_4
M_r	485.1	485.1	485.1	485.1	485.1
Cell setting, space group	Monoclinic, $P12/c1$	Monoclinic, $P12/c1$	Monoclinic, $P12/c1$	Monoclinic, $P12/c1$	Monoclinic, $P12/c1$
Temperature (K)	293 (1)	250 (1)	200 (1)	150 (1)	100 (1)
a, b, c (Å)	7.6396 (12), 4.9447 (7), 9.3596 (4)	7.6303 (12), 4.9405 (7), 9.3547 (14)	7.6231 (12), 4.9370 (7), 9.3528 (14)	7.6140 (12), 4.9319 (7), 9.3470 (14)	7.6084 (13), 4.9291 (7), 9.3464 (15)
β (°)	111.427 (11)	111.395 (11)	111.386 (11)	111.371 (11)	111.371 (12)
V (Å^3)	329.13 (9)	328.35 (9)	327.76 (9)	326.86 (8)	326.41 (9)
Z	2	2	2	2	2
D_x (Mg m^{-3})	4.895	4.907	4.915	4.929	4.936
Radiation type	Mo $K\alpha$	Mo $K\alpha$	Mo $K\alpha$	Mo $K\alpha$	Mo $K\alpha$
μ (mm^{-1})	11.39	11.42	11.44	11.47	11.48
Crystal form, colour	Parallelepiped, dark blue	Parallelepiped, dark blue	Parallelepiped, dark blue	Parallelepiped, dark blue	Parallelepiped, dark blue
Crystal size (mm)	0.24 × 0.21 × 0.15	0.24 × 0.21 × 0.15	0.24 × 0.21 × 0.15	0.24 × 0.21 × 0.15	0.24 × 0.21 × 0.15
Data collection					
Diffractometer	Stoe IPDS 2	Stoe IPDS 2	Stoe IPDS 2	Stoe IPDS 2	Stoe IPDS 2
Data collection method	Rotation, ω-scans	Rotation, ω-scans	Rotation, ω-scans	Rotation, ω-scans	Rotation, ω-scans
Absorption correction	Numerical	Numerical	Numerical	Numerical	Numerical
T_{min}	0.09	0.09	0.09	0.09	0.09
T_{max}	0.19	0.19	0.19	0.19	0.19
No. of measured, independent and observed reflections	5391, 1132, 1031	5369, 1125, 1025	5359, 1122, 1025	5337, 1119, 1021	5334, 1119, 1027
Criterion for observed reflections	$I>2\sigma(I)$	$I>2\sigma(I)$	$I>2\sigma(I)$	$I>2\sigma(I)$	$I>2\sigma(I)$
R_{int}	0.045	0.044	0.043	0.042	0.038
θ_{max} (°)	32.17	32.17	32.17	32.17	32.17
Refinement					
Refinement on	F^2	F^2	F^2	F^2	F^2
$R[F^2>2\sigma(F^2)]$, $wR(F^2)$, S	0.023, 0.040, 1.45	0.022, 0.038, 1.41	0.022, 0.038, 1.46	0.020, 0.036, 1.38	0.021, 0.035, 1.46
No. of reflections	1132	1125	1122	1119	1119
No. of parameters	66	66	66	66	66
H-atom treatment	No H atoms present	No H atoms present	No H atoms present	No H atoms present	No H atoms present
Weighting scheme	$w = 1/[\sigma^2(F_o^2) + (0.010P)^2]$, where $P = (F_o^2 + 2F_c^2)/3$	$w = 1/[\sigma^2(F_o^2) + (0.010P)^2]$, where $P = (F_o^2 + 2F_c^2)/3$	$w = 1/[\sigma^2(F_o^2) + (0.010P)^2]$, where $P = (F_o^2 + 2F_c^2)/3$	$w = 1/[\sigma^2(F_o^2) + (0.010P)^2]$, where $P = (F_o^2 + 2F_c^2)/3$	$w = 1/[\sigma^2(F_o^2) + (0.010P)^2]$, where $P = (F_o^2 + 2F_c^2)/3$
$(\Delta/\sigma)_{max}$	< 0.0001	< 0.0001	< 0.0001	< 0.0001	< 0.0001
$\Delta\rho_{max}$, $\Delta\rho_{min}$ (e Å^{-3})	0.80, −0.88	0.72, −0.76	0.83, −0.77	0.69, −0.78	0.77, −0.81
Extinction method	*SHELXL*	*SHELXL*	*SHELXL*	*SHELXL*	*SHELXL*
Extinction coefficient	0.0104 (5)	0.0087 (7)	0.0077 (6)	0.0078 (7)	0.0084 (7)

2. Experimental

2.1. Crystal growth

BaV_4O_9 single crystals were grown by a flux method. A salt mixture of LiCl, RbCl and $BaCl_2$ was first prepared by drying the components separately at 413 K and mixing them in the molar ratio 2:1:1. VO_2 powder was then added to the mixture in the flux:VO_2 mass ratio 10:1. The mixture was ground in an agate mortar, placed in an Al_2O_3 crucible and dried again because of the hygroscopic properties of $BaCl_2$. The crucible was then placed into a glass test tube, which was kept open and placed in a glass gas-washing bottle. The sample was heat-treated at 713 K for 24 d in a vertical tube furnace and then slowly cooled down to room temperature. During the growth process, argon gas (Ar 5.0) was flushed through the bottle to keep oxygen away and thus avoid the oxidation of the V^{4+} ions to the non-magnetic V^{5+} ions. Among the crystallized flux material, which also precipitated on the inner side of the test tube, small dark blue BaV_4O_9 single crystals could be found and isolated.

2.2. Single-crystal X-ray diffraction

Temperature-dependent single-crystal X-ray diffraction measurements were performed on a two-circle imaging plate diffractometer (Stoe-IPDS-II, Mo $K\alpha$ radiation, tube setting 50 kV and 25 mA, pyrolytic graphite monochromator). The diffractometer was equipped with a Cryostream cryogenic N_2 gas blower (80–300 K, accuracy 0.1 K). Five data sets (completeness >97%) were collected at 293, 250, 200, 150 and

Table 2
BaV_4O_9: environment of the V atoms (293 K).

V1—O2	1.7209 (19)	$O4^{i}$—V1—O2	102.18 (9)
V1—$O4^{i}$	1.9206 (20)	O3—V1—O2	95.44 (9)
V1—O3	1.9791 (18)	O5—V1—O2	98.69 (7)
V1—O5	1.9932 (14)	$O3^{ii}$—V1—O2	88.67 (9)
V1—$O3^{ii}$	2.0345 (20)	$O4^{ii}$—V1—O2	174.18 (9)
V1—$O4^{ii}$	2.0743 (19)	O3—V1—$O4^{i}$	94.97 (8)
V1—$V2^{i}$	2.8120 (7)	O5—V1—$O4^{i}$	85.45 (9)
V1—$V1^{ii}$	2.9870 (9)	$O3^{ii}$—V1—$O4^{i}$	169.15 (8)
V1—V2	2.9882 (7)	$O4^{ii}$—V1—$O4^{i}$	82.58 (8)
V1—$V1^{v}$	3.0035 (9)	O5—V1—O3	165.46 (6)
V1—$V2^{ii}$	3.2050 (7)	$O3^{ii}$—V1—O3	83.83 (8)
V1—$V1^{vi}$	3.5038 (11)	$O4^{ii}$—V1—O3	80.71 (8)
V1—$V2^{vii}$	3.5107 (8)	$O3^{ii}$—V1—O5	93.02 (8)
V1—$V2^{viii}$	3.6613 (8)	$O4^{ii}$—V1—O5	84.94 (6)
V1—$V2^{vi}$	3.7984 (8)	$O3^{ii}$—V1—$O4^{i}$	86.59 (8)
V2—O1	1.6188 (21)	O4—V2—O1	106.40 (10)
V2—O4	1.9521 (18)	O2—V2—O1	97.03 (10)
V2—O2	1.9781 (21)	$O5^{iii}$—V2—O1	108.83 (10)
V2—$O5^{iii}$	1.9968 (20)	$O3^{iv}$—V2—O1	101.07 (9)
V2—$O3^{iv}$	2.0084 (19)	$O3^{ii}$—V2—O1	172.76 (10)
V2—$O3^{ii}$	2.2765 (19)	O2—V2—O4	90.11 (8)
V2—$V2^{vi}$	2.8108 (10)	$O5^{iii}$—V2—O4	84.53 (6)
V2—$V1^{iii}$	2.8120 (7)	$O3^{iv}$—V2—O4	152.45 (8)
V2—V1	2.9882 (7)	$O3^{ii}$—V2—O4	76.34 (7)
V2—$V1^{ii}$	3.2050 (7)	$O5^{iii}$—V2—O2	154.08 (8)
V2—$V1^{iv}$	3.5107 (8)	$O3^{iv}$—V2—O2	88.67 (8)
V2—$V1^{ix}$	3.6613 (8)	$O3^{ii}$—V2—O2	76.14 (7)
V2—$V1^{vi}$	3.7984 (8)	$O3^{iv}$—V2—$O5^{iii}$	84.64 (7)
		$O3^{ii}$—V2—$O5^{iii}$	77.95 (7)
		$O3^{ii}$—V2—$O3^{iv}$	76.65 (8)

Symmetry codes: (i) $x, y-1, z$; (ii) $-x+1, -y+1, -z+1$; (iii) $x, y+1, z$; (iv) $x, -y+1, z-\frac{1}{2}$; (v) $x, y-1, z$; (vi) $-x+1, y, -z+\frac{1}{2}$; (vii) $x, -y+1, z+\frac{1}{2}$; (viii) $-x+1, y-1, -z+\frac{1}{2}$; (ix) $-x+1, y+1, -z+\frac{1}{2}$.

100 K. For each temperature, the data were collected with a crystal–detector distance of 8 cm, an exposure time of 4 min per frame, an ω scan between 0 and 180° for $\varphi = 0°$ and an ω scan between 0 and 90° for $\varphi = 70°$, with the rotation step $\Delta\omega = 1.5°$ per frame. The lattice parameters and the intensities of the reflections were obtained with the program *X-AREA* (Stoe & Cie, 2002). Numerical absorption corrections *via* symmetry equivalents were performed using the programs *X-RED* and *X-SHAPE* (Stoe & Cie, 1996). The room-temperature structure was solved using direct methods with the program *SIR*2002 (Burla *et al.*, 2003). The refinements were performed with the program *SHELXL*97 (Sheldrick, 1997), as implemented in the program suite *WinGX*, Version 1.64.05 (Farrugia, 1999). Details are summarized in Table 1. The monoclinic thermal expansion coefficients were calculated from the fitted temperature dependences of the cell parameters with a locally written Fortran program.

3. Results

3.1. Room-temperature structure of BaV_4O_9

BaV_4O_9 was found to crystallize in the monoclinic space group $P2/c$ (No. 13), with the room-temperature cell parameters a = 7.6396 (12), b = 4.9447 (7), c = 9.3596 (14) Å and β = 111.427 (11)°.

The structure of BaV_4O_9 consists of corrugated V_4O_9 zigzag layers separated by Ba^{2+} ions (Fig. 1). The Ba^{2+} ions, located on the twofold rotation axes at $(0, y, \frac{1}{4})$, are 12-fold coordinated by O atoms and form slightly distorted BaO_{12} anticuboctahedra, with Ba—O distances ranging between 2.750 (2) and 3.225 (2) Å. The V^{4+} ions occupy two non-equivalent general positions. Their coordination polyhedra are distorted VO_6 octahedra, with distinctly different distortions and linkages to each other (Table 2, Fig. 2): The $V1O_6$ octahedra share edges with other $V1O_6$ and $V2O_6$ octahedra to form V_4O_{12} double chains along the b direction; these chains are in turn linked *via* face-sharing $V2O_6$ octahedra to form the V_4O_9 layers. The O atoms occupy general positions, except for the O5 atom, lying on the twofold rotation axis at $(\frac{1}{2}, y, \frac{1}{4})$.

The shortest bond of the $V1O_6$ octahedron, V1—O2, is not a typical vanadyl bond: The O2 atom belongs both to the $V1O_6$ and $V2O_6$ octahedra. The opposite *trans* (apex) V1—$O4^{ii}$ bond is not much longer than the *cis* (equatorial) V1—O bonds; within the equatorial plane, we observe that the *cis* V1—$O4^{i}$ bond is significantly smaller than the other three. The $V1^{4+}$ ion and the O2, $O4^{i}$ apex atoms are roughly aligned in the (*ab*) plane and the O2—V1—O4 direction forms an angle of 25.0 (1)° with *a*. The $V1^{4+}$ ion does not exactly lie at the centre of the octahedron in the equatorial plane, but is slightly displaced towards the apex and *cis* ligands O2 and $O4^{i}$. Since the only cation neighbour of the O1 atom is $V2^{4+}$, the V2—O1 vanadyl bond of the $V2O_6$ octahedron is much closer to the usually measured value of 1.59 Å (Schindler *et al.*, 2000) and as a consequence, the *trans* V2—$O3^{ii}$ bond is longer. This

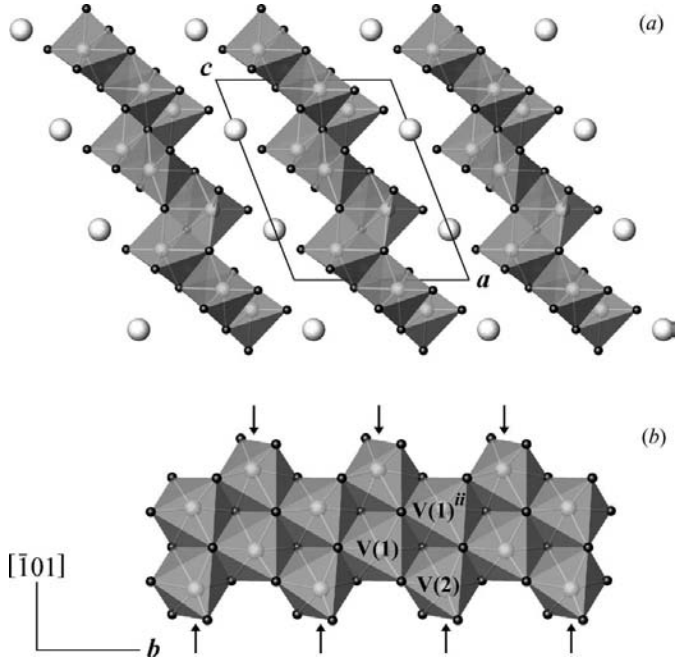

Figure 1
Room-temperature structure of BaV_4O_9. (*a*) Projection onto the *ac* plane. The VO_6 octahedra are represented in grey and the Ba^{2+} ions by the white spheres separating the layers. (*b*) Projection of a V_4O_{12} chain (parallel to the *b* direction) onto the plane containing **b** and [$\bar{1}$01]. The arrows point to the face-sharing $V2O_6$ octahedra linking two V_4O_{12} chains. See the caption to Table 2 for the symmetry codes.

octahedron also possesses a smaller V2—O4 *cis* equatorial bond length compared with the other three. The $V2^{4+}$ ion lies closer to the centre of the pyramid formed by the vanadyl and equatorial ligands than to the centre of the octahedron; however, the bond valence attached to the *trans* V2—$O3^{ii}$ bond is not negligible and justifies considering $O3^{ii}$ as the sixth ligand of V2. The vanadyl and *trans* bonds of the $V2O_6$ octahedron are almost parallel to the direction formed by the *trans* bonds of the $V1O_6$ octahedron.

The V_4O_9 zigzag layers can be described as consisting of V_4O_{12} double chains parallel to *b*, where the $V1O_6$ octahedra share equatorial edges with other $V1O_6$ octahedra and non-equatorial edges with the $V2O_6$ octahedra (Fig. 1*b*). Within such a chain, the V^{4+} ions form quasi-equilateral triangles, with the angles V1—V2—$V1^{ii}$ = 57.55 (2)°, V2—$V1^{ii}$—V1 = 57.58 (2)° and $V1^{ii}$—V1—V2 = 64.87 (2)°, so that unless there exist some relatively strong magnetic interactions between the double chains, frustration should play an important role in the properties of BaV_4O_9. It should be noted that an inversion center lies between V1 and $V1^{ii}$ and thus no Dzyaloshinsky–Moriya interaction can exist between these two ions (Dzyaloshinsky, 1958; Moriya, 1960). The V_4O_{12} chains are linked to each other *via* face-sharing $V2O_6$ octahedra: The environments of the $V1^{4+}$ and $V2^{4+}$ ions are quantitatively very different. The distinction between the two V sites is also seen by considering the possible V^{4+}–V^{4+} magnetic interactions within a V_4O_9 layer: The $V2^{4+}$ ion possesses fewer vanadium neighbours than $V1^{4+}$ (Table 2, Fig. 3). It is noteworthy that although the V^{4+} sublattice resembles a 1/5-depleted triangular framework, the vacant site between two $V1^{4+}$ cations is too small [V1—$V1^{vi}$ = 3.5038 (11) Å] to accommodate an additional V^{4+} cation.

Although the chemical formula of the title compound is reminiscent of CaV_4O_9 and the metastable phase SrV_4O_9, its crystal structure is very different. Both CaV_4O_9 and SrV_4O_9 crystallize in the tetragonal space group $P4/n$ (No. 85) and consist of edge-sharing VO_5 tetragonal pyramids, alternately pointing up and down the *c* direction, forming flat layers separated by the eightfold-coordinated alkaline earth ions. The V^{4+} ions lie on equivalent positions. In the neighbourhood of a VO_5 pyramid, there are no further O atoms opposite the vanadyl bond that could be considered as part of an elongated VO_6 octahedron. The coordination polyhedron of the Ca^{2+} (or Sr^{2+}) ion is a tetragonal antiprism. Within the V_4O_9 layers, the V^{4+} ions form a 1/5-depleted Heisenberg square checkerboard lattice and both materials are spin-gap systems. Thus, consid-

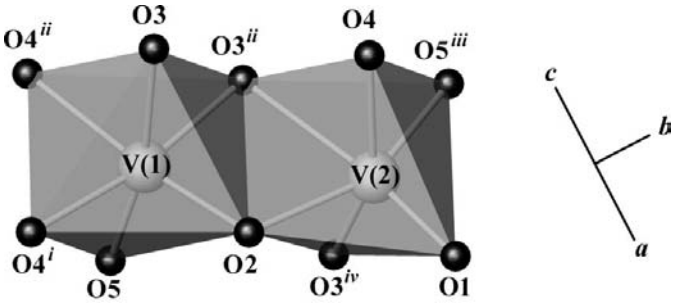

Figure 2
Room-temperature structure of BaV_4O_9: Environments of the V1 and V2 atoms. See caption of Table 2 for the symmetry codes.

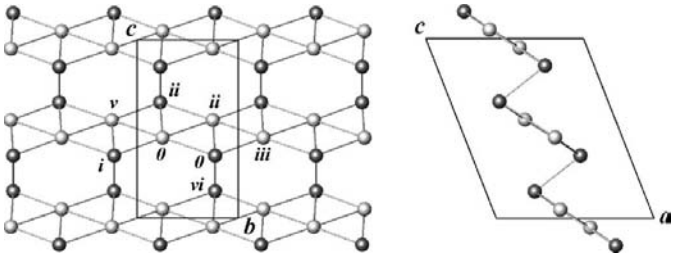

Figure 3
Projection of a corrugated V_4O_9 layer onto the *bc* plane (left) and onto the *ac* plane (right). The light grey spheres represent the $V1^{4+}$ ions and the dark grey spheres the $V2^{4+}$ ions. The O atoms have been omitted for clarity. See Table 2 for the symmetry codes.

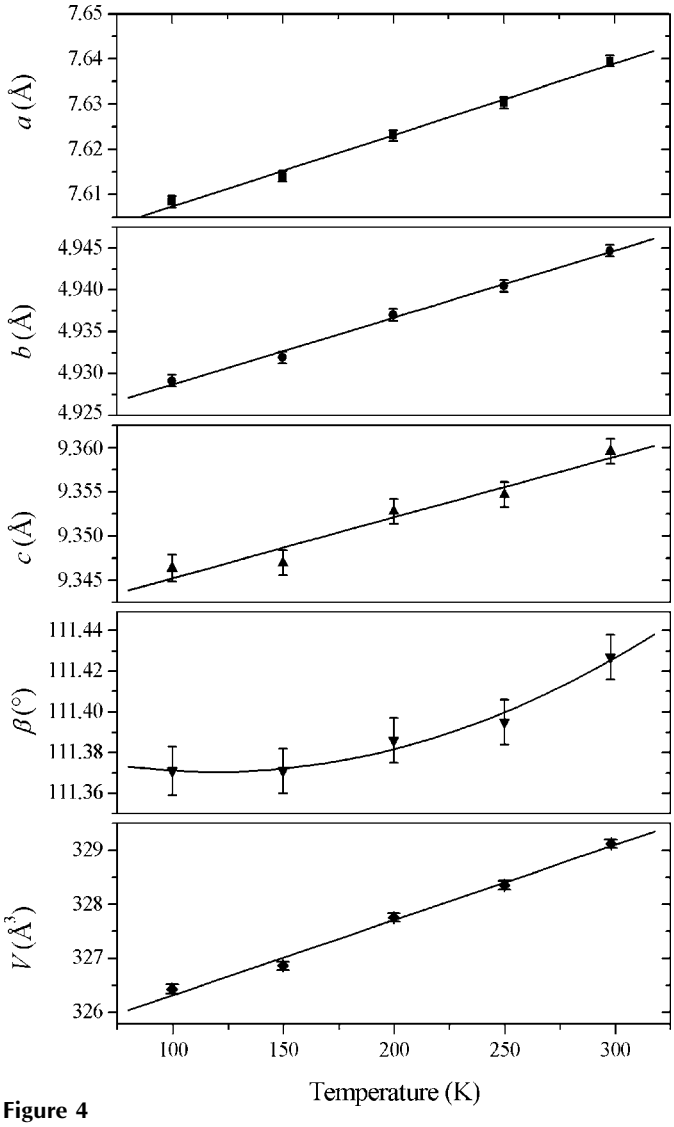

Figure 4
Temperature dependence of the cell parameters and volume of BaV_4O_9, obtained from single-crystal X-ray diffraction experiments. The linear fits for *a*, *b*, *c* and *V* and the second-order polynomial fit for β are guides to the eye.

ering the local geometries of the atomic coordinations as well as the linkage of the coordination polyhedra, the crystal structures of CaV_4O_9 and BaV_4O_9 are fundamentally unrelated to each other.

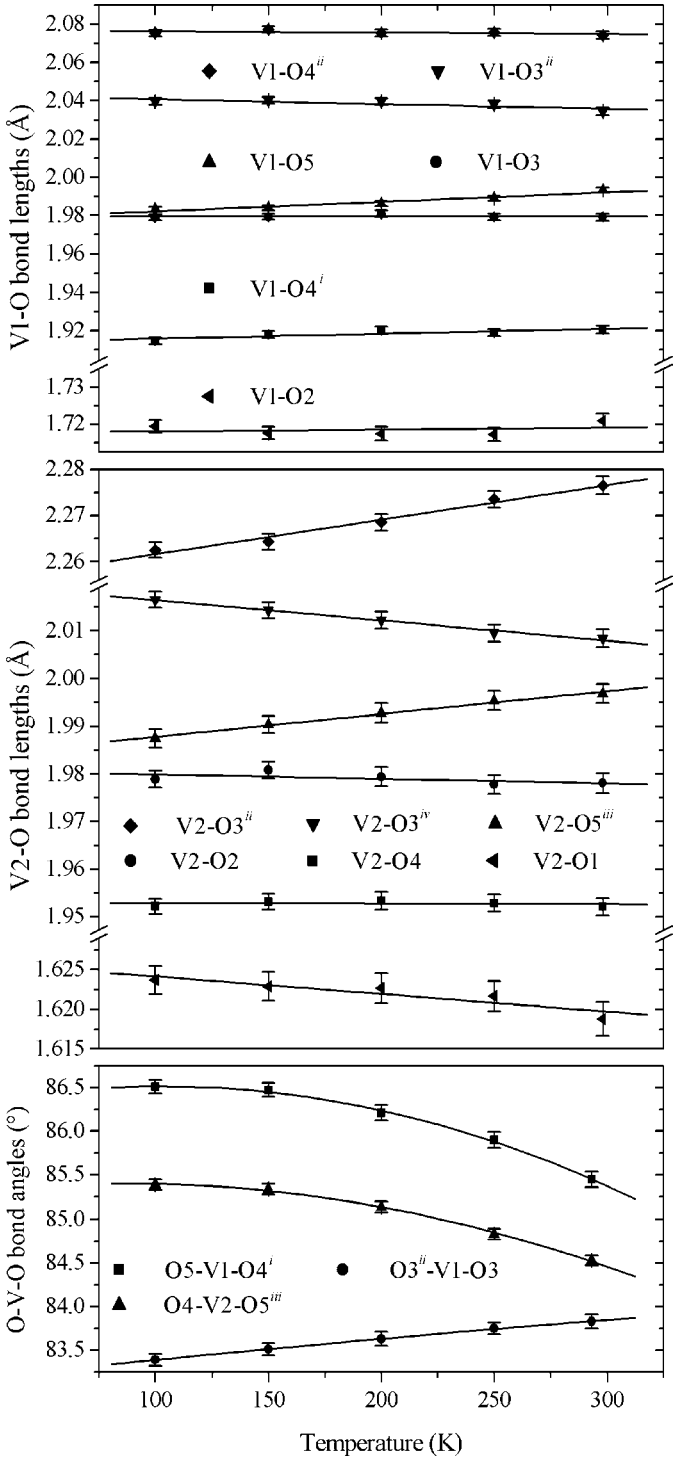

Figure 5
Evolution of the V—O bond lengths and some selected O—V—O bond angles as a function of temperature. The fits are used as guides to the eye. See caption of Table 2 for the symmetry codes.

3.2. Temperature-dependent evolution of BaV_4O_9

From room temperature down to 100 K, no evidence for a structural phase transition was observed (Fig. 4). The principal changes within the $V1O_6$ octahedron concern the O—V1—O bond angles: except for the *cis* V1—O5 bond, which increases slightly with increasing temperature, the lengths of the V1—O bonds remain constant within 3σ over the whole temperature range (Fig. 5). The three shortest bond lengths of the $V2O_6$ octahedron also remain constant within 3σ, but we observe quite large variations in the larger distances. In particular, the V2—O3^{iv} and V2—O5^{iii} *cis* bonds have comparable lengths at room temperature, but evolve linearly in opposite ways down to 100 K, thus distorting the equatorial plane of the octahedron.

The temperature dependences of the shortest $V^{4+}—V^{4+}$ distances seem at first rather complicated (Fig. 6). The V1—V1^{v} and V1—V2 distances increase linearly with increasing temperature, with slopes of $2.5\,(2) \times 10^{-5}$ and $1.7\,(2) \times 10^{-5}$ Å K^{-1}, respectively. The V1—V2^{i} and V2—V2^{vi} distances do not follow a linear trend, but increase quadratically, the absolute change in the V1—V2^{i} distance being almost three times larger than for V2—V2^{vi}. On the other hand, V1—V1^{ii} drastically decreases from 100 K, where it is longer than the V1—V1^{v} distance, up to 293 K where it becomes shorter than the V1—V2 distance.

These distances can generally be divided into three groups. The linearly increasing V1—V1^{v} and V1—V2 distances form an almost straight line more or less in the direction of the V_4O_{12} double chains, with a V1^{v}—V1—V2 angle of 174.31 (2)° at 100 K and 175.40 (3)° at 293 K. The V1—V1^{ii} and V1—V2^{i}

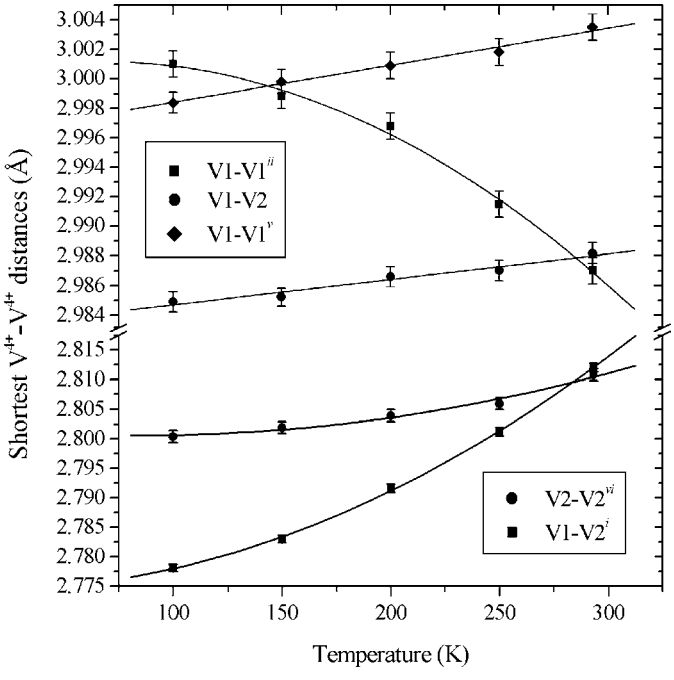

Figure 6
Evolution of the shortest V^{4+}–V^{4+} distances as a function of temperature. The fits are used as guides to the eye. See caption of Table 2 for the symmetry codes.

Table 3
Top: coefficients α_{ij} (10^{-6} K^{-1}) of the thermal expansion tensor of BaV_4O_9; bottom: eigenvalues α_1 and α_3 in 10^{-6} K^{-1} ($\alpha_2 = \alpha_{22}$) and angles between the eigenvectors $\boldsymbol{a}_1$, $\boldsymbol{a}_3$ of the thermal expansion tensor of BaV_4O_9 and the orthogonal crystal axes $\mathbf{a}^*$, $\mathbf{b}$ and $\mathbf{c}$.

ΔT (K)	α_{11}	α_{22}	α_{33}	α_{13}
293–250	21 (1)	16 (1)	7 (1)	−7.2 (8)
250–200	19 (1)	16 (1)	7 (1)	−5.8 (8)
200–150	18 (1)	16 (1)	7 (1)	−4.3 (8)
150–100	17 (1)	16 (1)	7 (1)	−2.8 (8)

			Eigenvector angles (°)		
ΔT (K)	$\boldsymbol{a}_i$	α_i	$\angle(\boldsymbol{a}_i, \boldsymbol{a}^*)$	$\angle(\boldsymbol{a}_i, \boldsymbol{b})$	$\angle(\boldsymbol{a}_i, \boldsymbol{c})$
293–250	$\boldsymbol{a}_1$	4 (1)	62 (3)	90	28 (3)
	$\boldsymbol{a}_3$	21 (1)	152 (3)	90	62 (3)
250–200	$\boldsymbol{a}_1$	5 (1)	67 (3)	90	23 (3)
	$\boldsymbol{a}_3$	21 (1)	157 (3)	90	67 (3)
200–150	$\boldsymbol{a}_1$	6 (1)	72 (3)	90	18 (3)
	$\boldsymbol{a}_3$	21 (1)	162 (3)	90	72 (3)
150–100	$\boldsymbol{a}_1$	7 (1)	79 (3)	90	11 (3)
	$\boldsymbol{a}_3$	21 (1)	169 (3)	90	79 (3)

distances, behaving quadratically with temperature, form the second pair along the direction of the chain, with a V1^{ii}—V1—V2^{i} angle of 176.09 (3)° at 100 K and 176.72 (3)° at 293 K. Since V1—V1^{ii} decreases more slowly than V1—V2^{i} increases, the whole chain is denser along the *b* direction at lower temperatures. Thirdly, we have the short V2—V2^{vi} distance involved in the face-sharing $V2O_6$ octahedra, linking two V_4O_{12} double chains. Also represented in Fig. 3 is the larger V1—V2^{ii} distance, which points perpendicular to the chains and increases slightly with increasing temperature.

The temperature dependences of the V^{4+}—V^{4+} distances probably arise from the combination of thermal expansion and magnetic interactions, and are related to the changes in the VO_6 octahedra. The $V1O_6$ and $V1^{ii}O_6$ octahedra share edges *via* the O3 and O3^{ii} atoms; the non-linear decrease of the V1—V1^{ii} distance is explained by or explains the linear increase of the *cis–cis* O3—V1—O3^{ii} bond angle (bottom part of Fig. 5), which further shears the equatorial plane of the $V1O_6$ octahedron at lower temperatures. Similarly, the increase of the V1—V1^{v} distance is related to the decrease of the *cis–trans* O4^{i}—V1—O4^{ii} bond angle. The $V1O_6$ and $V2^{i}O_6$ octahedra share edges *via* the O4^{i} and O5 atoms: The non-linear increase of the V1—V2^{i} distance with increasing temperature coincides with the simultaneous decreases in the *cis–cis* O4^{i}—V1—O5 and *cis–cis* O4—V2—O5^{iii} bond angles. In the case of the face-sharing $V2O_6$ and $V2^{vi}O_6$ octahedra, the increase of the V2—V2^{vi} distance is better understood by considering the temperature dependence of the V2—O bond lengths. Owing to the twofold rotation axis at $(\frac{1}{2}, y, \frac{1}{4})$ between V2 and V2^{vi}, the variations of the *trans* V2—O3^{ii} and *cis* V2—O3^{iv} bond lengths compensate each other and only the increasing *cis* V2—O5^{iii} bond length has an influence on the V2—V2^{vi} distance.

3.3. Thermal expansion tensor

The cell parameters *a*, *b* and *c* decrease linearly with temperature, the highest absolute change being observed along the *a* direction (Fig. 4). The Lagrangian components of the thermal expansion tensor α_{11}, α_{22}, α_{33} and α_{13} were obtained for the conventional orthonormal basis $e_3 \parallel c$, $e_2 \parallel b^*$ and $e_1 \parallel e_2 \times e_3$ (*i.e.* $e_3 \parallel c$, $e_2 \parallel b$ and $e_1 \parallel a^*$ for a monoclinic system) using the following relationships (Knight *et al.*, 1999), with linear functions for *a*, *b*, *c* and a second-order polynomial function for β

$$\alpha_{11}(T) = \frac{1}{a_0 \sin\beta_0}\left(\sin\beta\frac{\mathrm{d}a}{\mathrm{d}T} + a\cos\beta\frac{\mathrm{d}\beta}{\mathrm{d}T}\right)$$
$$\alpha_{22}(T) = \frac{1}{b_0}\frac{\mathrm{d}b}{\mathrm{d}T}$$
$$\alpha_{33}(T) = \frac{1}{c_0}\frac{\mathrm{d}c}{\mathrm{d}T}$$
$$\alpha_{13}(T) = \frac{1}{a_0}\frac{\mathrm{d}a}{\mathrm{d}T}\left(\frac{1}{\sin 2\beta_0} - \frac{\sin\beta}{2\cos\beta_0}\right) - \frac{a\cos\beta}{2a_0\cos\beta_0}\frac{\mathrm{d}\beta}{\mathrm{d}T} - \frac{\cot\beta_0}{2c_0}\frac{\mathrm{d}c}{\mathrm{d}T}.$$

In each temperature range, all the three principal components of the thermal expansion tensor are positive (Table 3): The representation quadric is a triaxial ellipsoid. We observe that the ratio between the smallest and largest eigenvalues (α_1 and α_3, respectively) decreases slightly with temperature, but the anisotropy of the tensor remains very pronounced. As the temperature decreases, the eigenvectors α_1 and α_3 of the $[\alpha_{ij}]$ tensor tend to become parallel to **c** and the reciprocal vector $\mathbf{a}^*$, respectively (Fig. 7), while the α_{13} component decreases. However, this behavior is not accompanied by a decrease of the β monoclinic angle towards 90°, so the possibility of a simultaneous phase transition towards an orthorhombic phase

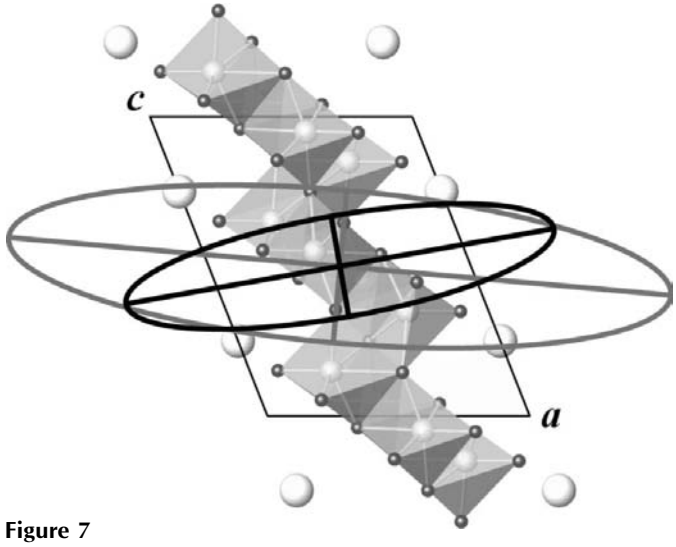

Figure 7
Temperature-dependent rotation of the eigenvectors $\boldsymbol{e}_1$ and $\boldsymbol{e}_3$ of the thermal expansion tensor of BaV_4O_9: projection of the ellipsoid onto the *ac* plane. The grey ellipse represents the room-temperature tensor and the black ellipse the low-temperature tensor (125 K).

is ruled out. Instead, the rotation of the principal axes of the thermal expansion tensor directly reflects the change in the anisotropy of the anharmonicity within the crystal upon cooling. No obvious relationship between the temperature dependence of the crystal structure of BaV_4O_9 and the evolution of the thermal expansion tensor could be found.

4. Conclusions

We have synthesized a new compound in the Ba–V–O system, chemically similar to CaV_4O_9 and SrV_4O_9, but with a novel layered structure. Further preparative work is in progress to synthesize enough material for magnetic measurements.

References

Azuma, M., Hiroi, Z., Takano, M., Ishida, K. & Kitaoka, Y. (1994). *Phys. Rev. Lett.* **73**, 3463–3466.

Bednorz, J. G. & Müller, K. A. (1986). *Z. Phys. B Condens. Matter*, **64**, 189–193.

Bouloux, J.-C. & Galy, J. (1973). *Acta Cryst.* B**29**, 1335–1338.

Burla, M. C., Camalli, M., Carrozzini, B., Cascarano, G. L., Giacovazzo, C., Polidori, G. & Spagna, R. (2003). *J. Appl. Cryst.* **36**, 1103.

Dzyaloshinsky, I. (1958). *J. Phys. Chem. Solids*, **4**, 241–255.

Farrugia, L. J. (1999). *J. Appl. Cryst.* **32**, 837–838.

Hase, M., Terasaki, I. & Uchinokura, K. (1993). *Phys. Rev. Lett.* **70**, 3651–3654.

Johnston, D. C., Johnson, J. W., Goshorn, D. P. & Jacobson, A. J. (1987). *Phys. Rev. B*, **35**, 219–222.

Kageyama, H., Yoshimura, K., Stern, R., Mushnikov, N. V., Onizuka, K., Kato, M., Kosuge, K., Slichter, C. P., Goto, T. & Ueda, Y. (1999). *Phys. Rev. Lett.* **82**, 3168–3171.

Knight, K. S., Stretton, I. C. & Schofield, P. F. (1999). *Phys. Chem. Miner.* **26**, 477–483.

Liu, G. & Greedan, J. E. (1993). *J. Solid State Chem.* **103**, 228–239.

Liu, G. & Greedan, J. E. (1994*a*). *J. Solid State Chem.* **108**, 371–380.

Liu, G. & Greedan, J. E. (1994*b*). *J. Solid State Chem.* **110**, 274–289.

Liu, G. & Greedan, J. E. (1995). *J. Solid State Chem.* **115**, 174–186.

Matsuda, M. & Katsumata, K. (1996). *Phys. Rev. B*, **53**, 12201–12205.

Moriya, T. (1960). *Phys. Rev.* **120**, 91–98.

Oka, Y., Yao, T. & Yamamoto, N. (1995). *J. Solid State Chem.* **117**, 407–411.

Oka, Y., Yao, T., Yamamoto, N., Ueda, M. & Maegawa, S. (2000). *J. Solid State Chem.* **149**, 414–418.

Schindler, M., Hawthorne, F. C. & Baur, W. H. (2000). *Chem. Mater.* **12**, 1248–1259.

Sheldrick, G. M. (1997). *SHELXL*97. University of Göttingen, Germany.

Stoe & Cie (1996). *X-SHAPE and X-RED*. Stoe and Cie GesmbH, Germany.

Stoe & Cie (2002). *X-AREA*. Stoe and Cie GesmbH, Germany.

Taniguchi, S., Nishikawa, T., Yasui, Y., Kobayashi, Y., Sato, M., Nishioka, T., Kontani, M. & Sano, K. (1995). *J. Phys. Soc. Jpn*, **64**, 2758–2761.

Ueda, Y. (1998). *Chem. Mater.* **10**, 2653–2664.

Wang, X., Liu, L., Bontchev, R. & Jacobson, A. J. (1998). *Chem. Commun.* pp. 1009–1010.